

ARTICLE TEMPLATE

Bayesian Spike Train Inference via Non-Local Priors

Abhisek Chakraborty

Department of Statistics, Texas A&M University, College Station, TX 77843, USA

ARTICLE HISTORY

Compiled July 21, 2023

ABSTRACT

Advances in neuroscience have enabled researchers to measure the activities of large numbers of neurons simultaneously in behaving animals. We have access to the fluorescence of each of the neurons which provides a first-order approximation of the neural activity over time. Determining a neuron's exact spike from this fluorescence trace constitutes an active area of research within the field of computational neuroscience. We propose a novel Bayesian approach based on a mixture of half-non-local prior densities and point masses for this task. Instead of a computationally expensive MCMC algorithm, we adopt a stochastic search-based approach that is capable of taking advantage of modern computing environments often equipped with multiple processors, to explore all possible arrangements of spikes and lack thereof in an observed spike train. It then reports the highest posterior probability arrangement of spikes and posterior probability for a spike at each location of the spike train. Our proposals lead to substantial improvements over existing proposals based on L_1 regularization, and enjoy comparable estimation accuracy to the state-of-the-art L_0 proposal, in simulations, and on recent calcium imaging data sets. Notably, contrary to optimization-based frequentist approaches, our methodology yields automatic uncertainty quantification associated with the spike-train inference.

KEYWORDS

Calcium imaging; Bayesian shrinkage; Non local prior; Stochastic search; Maximum a posteriori inference.

1. Introduction

When a neuron fires, calcium floods the cell. To measure this influx of calcium inside the cells, calcium imaging techniques make use of fluorescent calcium indicator molecules (Theis (2016), Rupprecht (2021)). Thus, a neuron's calcium fluorescence trace can be seen as a first-order approximation of its activity level over time. However, typically fluorescence trace is not particularly interesting on its own. Instead, it is used to determine the underlying activity level, that is, the specific times at which the neuron spiked. Inference of spike times from fluorescence traces amounts to a challenging deconvolution problem, and research in computational neuroscience has been focused on solving it (Vogelstein (2009); Vogelstein (2010); Pnevmatikakis EA (2016); Friedrich and Paninski (2016); Theis (2016); Friedrich and Paninski (2016); Friedrich (2017); Jewell et al. (2019), Rupprecht (2021)).

We will work with an auto-regressive model for calcium dynamics that has been taken into consideration by several authors in the recent literature (Vogelstein (2010);

Pnevmatikakis EA (2016); Friedrich and Paninski (2016); Friedrich (2017), Jewell et al. (2019)). We closely follow the notations introduced in Jewell et al. (2019). Our model assumes that y_t , the fluorescence at the t -th time-step, is a noisy realization of c_t , the unobserved underlying calcium concentration at the t -th time-step. A p -th-order auto-regressive process governs the calcium concentration decay in the absence of a spike at the t -th time-step ($s_t = 0$). The calcium concentration rises, nevertheless, if a spike occurs at the t -th time-step ($s_t > 0$). Thus,

$$\begin{aligned} y_t &= \beta_0 + \beta_1 c_t + \varepsilon_t, & \varepsilon_t &\stackrel{ind}{\sim} \text{N}(0, \sigma^2), & t &= 1, \dots, T; \\ c_t &= \sum_{i=1}^p \gamma_i c_{t-i} + s_t, & t &= p+1, \dots, T; \end{aligned} \tag{1}$$

In 1, the quantities $\gamma_1, \dots, \gamma_p$ are the parameters in the auto-regressive model. Note that the quantity y_t in 1 is observed; all other quantities are unobserved. Since we would like to know whether a spike occurred at the t -th time-step, the parameter of interest is $s_t = c_t - \sum_{i=1}^p \gamma_i c_{t-i} \geq 0$. For ease of exposition, following common practice in the literature Jewell et al. (2019), we assume $\beta_0 = 0$ and $\beta_1 = 1$ in 1. This assumption is made without loss of generality, since β_0 and β_1 can be estimated from the data, and the observed fluorescence y_1, \dots, y_T centered and scaled accordingly. Further, primarily we focus on the AR(1) case, where $\gamma_1 = \gamma \in (0, 1)$ and $\gamma_i = 0$ for $i \geq 2$. Notably, calcium imaging data sets are usually in high dimensions where the spike train is observed for few thousand time-points. Spikes, however, only show up at a select few time points. In other words, the majority of the entries in $(s_1, \dots, s_T)'$ are zero. This is the sparsity assumption that we need to enforce, and consequently the major goal is to locate the time-points with $s_t = c_t - \gamma c_{t-1} > 0$, equivalently, the time-points with a spike.

Many popular penalized likelihood techniques that were first developed for linear regression have also been used to spike train inference. Vogelstein (2010) proposed to impose the LASSO penalty (Tibshirani (1996)) on s_2, \dots, s_T . Friedrich and Paninski (2016) and Friedrich (2017) instead consider a closely-related problem that results from including an additional LASSO penalty for the initial calcium concentration c_1 . More recently, Jewell et al. (2019) proposed to put the L_0 penalty on s_2, \dots, s_T , and developed an algorithm to obtain the exact global solution for the resulting optimization problem. Further, to ensure computation ease, they solve the optimization problem after removing the positivity constraint $s_t \geq 0$. In reality, there isn't much of a difference between including and disregarding the positivity requirement because the solutions for real-world applications typically are the same for appropriate decay rate γ . This cutting-edge method Jewell et al. (2019) guarantees significant advantages in the spike detection task over its $L1$ regularization-based rivals.

A few Bayesian solutions have also been put out to deal with this issue. Vogelstein (2010) proposed a non-negative deconvolution filter to infer the approximately most likely spike train of each neuron, given the fluorescence observations. Pnevmatikakis EA (2013) proposed discrete time algorithms to find the existence of a spike at each time bin using Gibbs methods, as well as continuous time algorithms that sample over the number of spikes and their locations at an arbitrary resolution using Metropolis-Hastings methods for point processes. Friedrich and Paninski (2016) suggested spike inference from calcium imaging data using a sequential monte carlo method (Moral (2006)). For a more detailed review, we refer to the recent thesis (Linderman et al. (2016)). Notably, Bayesian methods are less utilized than their

frequentist counterparts, as the computational load of the associated Monte Carlo Markov Chain (MCMC) procedures often renders these approaches infeasible. This leads to the question of whether it's possible to develop a reasonably fast Bayesian methodology that can outperform dominant frequentist algorithms.

In this paper, we propose a new approach for this task based on a novel application of a mixture prior on spike variables that has a point mass at zero and a half non local density (Johnson and Rossell (2010)), in the auto-regressive model for calcium dynamics. These non local priors, although introduced in the context of Bayesian hypotheses testing, have proven useful in varied setups, e.g, high-dimensional linear regression (Johnson and Rossell (2012); Shin et al. (2018)), high-dimensional logistic regression (Nikooienejad et al. (2016)), survival analysis (Nikooienejad (2020)), sequential inference (Pramanik et al. (2021)) etc. Here, we impose inverse moment prior or product exponential moment prior on $s_t, t = 2, \dots, T$, and report the arrangements of spikes and lack thereof with highest posterior probability. The computationally burdensome MCMC process is avoided by adapting a stochastic search based method (Shin et al. (2018)).

This article is structured as follows. In section 2, we introduce methodology based on a novel application of non-local prior densities. In section 3, we present elaborate and realistic simulation studies to compare the proposed methodology with the existing and state-of-the-art penalised likelihood methods. Section 4 presents the spike train inference of calcium imaging data sets. Finally, we conclude.

2. Methods

2.1. Model and Prior Specification

Suppose we observe a spike train of calcium concentrations $\mathbf{y} = \{y_i\}_{i=1}^T$ indexed by time t . We primarily work with the AR(1) model for calcium dynamics:

$$\begin{aligned} y_t &= \beta_0 + \beta_1 c_t + \varepsilon_t, & \varepsilon_t &\stackrel{ind}{\sim} \text{N}(0, \sigma^2), & t &= 1, \dots, T; \\ c_t &= \gamma c_{t-1} + s_t, & & & t &= 2, \dots, T; \end{aligned} \tag{2}$$

where we assume that $\beta_0 = 0$, $\beta_1 = 1$ without loss of generality. We formally define an *arrangement* of the spikes and lack thereof by $\mathbf{k} = \{k_1, k_2, \dots, k_j\}$ where $2 \leq k_1 < k_2 \dots < k_j \leq T$ such that $s_t > 0$ if $t \in \mathbf{k}$ and 0 otherwise. Next, we define a Bayesian hierarchical model in which $\pi(\mathbf{y} \mid s_{(\mathbf{k})}, c_{1:T})$ is the likelihood of $(s_{(\mathbf{k})}, c_{1:T})$ obtained from the model in 2, $\pi_{\mathbf{k}}(\cdot)$ is the prior on the spike variables $s_{(\mathbf{k})}$, $\pi_c(\cdot)$ is a compactly supported flat prior on $c_{1:T}$, and finally $p(\cdot)$ is the prior for arrangement \mathbf{k} . The posterior probability for arrangement \mathbf{j} according to the Bayes rule is expressed as

$$p(\mathbf{j} \mid \mathbf{y}) = \frac{p(\mathbf{j}) m_{\mathbf{j}}(\mathbf{y})}{\sum_{\mathbf{k} \in \mathcal{J}} p(\mathbf{k}) m_{\mathbf{k}}(\mathbf{y})}$$

where \mathcal{J} is the set of all possible arrangements and the marginal probability of the data under the arrangement \mathbf{j} is computed by

$$m_{\mathbf{j}}(\mathbf{y}) = \int \pi(\mathbf{y} \mid s_{(\mathbf{j})}) \pi_{\mathbf{j}}(s_{(\mathbf{j})}) \pi_c(c_{1:T}) ds_{(\mathbf{j})} dc.$$

Notably, the prior density for $\pi_{\mathbf{k}}(\cdot)$ and the prior on the arrangement space $p(\mathbf{j})$ impact the overall performance of the spike detection mechanism and the number of spikes in the resulting arrangement, and therefore we exercise ardent care in our choices of these priors.

First, we discuss the prior $p(\cdot)$ on the spike arrangement space. Note that, the events $\{t \in \mathbf{k}\}$, $t = 2, \dots, T$ can be modeled via independent Bernoulli trials. In particular, if we assume $P(t \in \mathbf{k}) = \theta \in (0, 1)$, then the resulting marginal probability for the arrangement \mathbf{k} becomes $\int_0^1 \theta^k (1 - \theta)^{T-1-k} \pi(\theta) d\theta$, where $\pi(\theta)$ is the prior on θ . A completely conjugate choice of $\pi(\theta)$ would be $\beta(a, b)$, and that yields

$$p(\mathbf{k}) = \int_0^1 \theta^k (1 - \theta)^{T-1-k} \pi(\theta) d\theta = \frac{\beta(a + k, b + T - 1 - k)}{\beta(a, b)}. \quad (3)$$

For most practical purposes, we suggest to choose $a = 1$ and $b = 1$ which ensures that we do not necessarily assign low prior probability to arrangements with many spikes.

Next, we focus on the prior specification on the spike variables s_t , $t = 2, \dots, T$. Here we put two-component mixture that has a spike at zero and a half-non-local density. In particular, we consider either of the two classes of half-non-local prior densities on \mathbb{R}^+ , obtained via restricting the non-local priors (Johnson and Rossell (2010), Johnson and Rossell (2012), Shin et al. (2018)) with full support on \mathbb{R} , as follows:

$$\pi(s) \propto s^{-(r+1)} \exp\left(-\frac{\tau}{s^2}\right), \quad s > 0, \quad [\text{Inverse moment prior (iMOM)}]; \quad (4)$$

$$\pi(s) \propto s^{-(r+1)} \exp\left(-\frac{s^2}{2\sigma^2\tau} - \frac{\tau}{s^2}\right), \quad s > 0, \quad [\text{Exponential moment prior (eMOM)}]. \quad (5)$$

Here the (τ, r) are prior hyper-parameters. While the hyper parameter r is comparable to the shape parameter in the inverse gamma distribution and controls the tail behavior of the density, the hyper parameter τ represents a scale parameter that affects the prior's dispersion around 0. Notably, large values of the spikes are not penalized by this prior, in contrast to the majority of penalized likelihood approaches. Consequently, it does not always impose harsh penalties on arrangements that have a lot of spikes. In general, we found that $r = 1$ and $\tau = 0.25$ are good default values. Finally, note that the model in 2 can be completely expressed by means of the minimal set of parameters $c_1, \sigma^2, s_{2:T}$. We complete our prior specification by putting a compactly supported non-informative prior on c_1 of the form

$$\pi_{(c)}(c_1) \sim \text{Unifrom}(0, c_{max}) \quad \text{where } c_{max} \text{ is large enough,} \quad (6)$$

and

$$\pi(\sigma^2) \equiv \text{Inverse-Gamma}(a_0, b_0). \quad (7)$$

So, the equations (2)-(7) complete our model and prior specification for the studying calcium dynamics.

2.2. Posterior Inference

Since we monitor the spike train over a huge number of time points, full posterior sampling with the current MCMC techniques is very costly and frequently not practicable. To overcome this problem, based on Shin et al. (2018), we suggest a scalable stochastic search strategy for quickly locating areas of high posterior probability and determining maximum a posteriori arrangement of spikes and absence of spikes. To that end, first note that $\hat{\mathbf{k}}$ denote the maximum a posteriori arrangement:

$$\hat{\mathbf{k}} = \arg \max_{\mathbf{k} \in \Gamma} \pi(\mathbf{k} | \mathbf{y}), \quad (8)$$

where Γ is the set of all arrangements assigned non-zero prior probability. However, we cannot ensure that a local maxima found by a deterministic search algorithm is the global maximum until we search all feasible arrangements in Γ because the optimization problem in (8) is NP-hard.

Stochastic Search Algorithms

In the context of model selection tasks, to overcome this problem, Hans et al. (2007) proposed a shotgun stochastic search algorithm in an attempt to identify the global maximum with high probability. This approach defines a neighbourhoods of the form $N(\mathbf{k}) = \{\Gamma^-, \Gamma^0, \Gamma^+\}$ where $\Gamma^- = \{\mathbf{k} \setminus j : j \in \mathbf{k}\}$, $\Gamma^+ = \{\mathbf{k} \cup j : j \in \mathbf{k}^c\}$ and $\Gamma^0 = \{(\mathbf{k} \setminus j) \cup l : j \in \mathbf{k}, l \in \mathbf{k}^c\}$, and proposed to the stochastic search **Algorithm 1**.

Algorithm 1 Shotgun Stochastic Search (SSS), Hans et al. (2007)

- (1) Choose an $\mathbf{k}^{(1)}$ and total number of iterations N .
 - (2) For $i \in \{1, \dots, N - 1\}$
 - (a) calculate $\pi(\mathbf{k} | \mathbf{y})$ for all $\mathbf{k} \in N(\mathbf{k}^{(i)})$,
 - (b) select $\mathbf{k}^-, \mathbf{k}^0$, and \mathbf{k}^+ from $\Gamma^-, \Gamma^0, \Gamma^+$ with probabilities $\pi(\cdot | \mathbf{y})$,
 - (c) select \mathbf{k} from $\{\mathbf{k}^-, \mathbf{k}^0, \mathbf{k}^+\}$ with probabilities $\{\pi(\mathbf{k}^- | \mathbf{y}), \pi(\mathbf{k}^0 | \mathbf{y}), \pi(\mathbf{k}^+ | \mathbf{y})\}$.
 - (3) Choose the arrangement with largest posterior probability among $\{\mathbf{k}^{(i)}, i = 1, \dots, N\}$.
-

Shotgun Stochastic Search is efficient in locating regions of high posterior probability in the arrangement space, but because it necessitates the assessment of marginal probabilities for arrangements in $\Gamma^-, \Gamma^0, \Gamma^+$ in each iteration, its computational cost is still significant. The largest computational expense is due to the evaluation of marginal likelihood for arrangements in Γ^0 since $|\Gamma^0| = |\mathbf{k}|(T - |\mathbf{k}|)$. In an attempt to remedy this issue, in the context of model selection exercises, Shin et al. (2018) proposed a simplified Shotgun Stochastic Search that only considers arrangements in Γ^-, Γ^+ which have cardinality $(T - |\mathbf{k}|)$ and $|\mathbf{k}|$, respectively. However, by ignoring Γ^0 in the sampling updates, we increase the likelihood that the algorithm will become trapped in a local maxima and make it less likely to explore the intriguing regions with high posterior probability. To solve this issue, a temperature parameter that is similar to simulated annealing was included, enabling the algorithm to explore a wider range of configurations.

Ignoring arrangements in Γ^0 undoubtedly reduces the computational burden of the Shotgun Stochastic Search algorithm. But when T is very large, computing the posterior probability for each iteration is still computationally expensive. To further alle-

viate this computational challenge, following Shin et al. (2018), we adapt ideas from Iterative Sure Independence Screening Fan (2008) and consider only those time-points which have a large correlation with the residuals of the current arrangement. To make it precise, first note that the model in 2 can be expressed as

$$\mathbf{y} = \Omega (c_1, s_2, \dots, s_T)' + \varepsilon$$

where $\mathbf{y} = (y_1, y_2, \dots, y_T)'$, $\varepsilon = (\varepsilon_1, \dots, \varepsilon_T)'$ and $\Omega = (\Omega_1, \Omega_2, \dots, \Omega_T)'$ is a $T \times T$ matrix of the form:

$$\begin{bmatrix} 1 & 0 & 0 & \dots & 0 \\ \gamma & 1 & 0 & \dots & 0 \\ \gamma^2 & \gamma & 1 & \dots & 0 \\ \gamma^3 & \gamma^2 & \gamma & \dots & 0 \\ \dots & \dots & \dots & \dots & \dots \\ \gamma^{T-1} & \gamma^{T-2} & \gamma^{T-3} & \dots & 1 \end{bmatrix}$$

where $\gamma \in (0, 1)$. We compute the quantities $r_{\mathbf{k}}' \Omega_j$, where $r_{\mathbf{k}}$ is the residual of arrangement \mathbf{k} , for $j = 1, \dots, T$, after iteration j of the modified algorithm, and then restrict attention to time-points for which $|r_{\mathbf{k}}' \Omega_j|$ is large (we assume that the columns of Γ have been standardized). This yields a scalable algorithm even when the number of time points T is large.

The resulting Simplified Shotgun Stochastic Search with Screening (S5) algorithm is described in **Algorithm 2**. In this algorithm, $S_{\mathbf{k}}$ is the union of time-points in \mathbf{k} and the top M time-points obtained by screening using the residuals from arrangement \mathbf{k} . So, the screened neighborhood of arrangement \mathbf{k} can be defined as $N_{\text{screen}}(\mathbf{k}) = \{\Gamma_{\text{screen}}^+, \Gamma^-\}$, where $\Gamma_{\text{screen}}^+ = \{\mathbf{k} \cup \{j\} : j \in \mathbf{k}^c \cap S_{\mathbf{k}}\}$. The adapted S5 algorithm only considers the addition of M new time-points in each iteration, which dramatically reduces the computational burden to construct Γ_{screen}^+ . In order to prevent re-evaluation and further improve computing performance, we keep the posterior probabilities of visited arrangements.

Algorithm 2 Simplified shotgun stochastic search algorithm with screening (S5), adapted from Shin et al. (2018)

- (1) Set a temperature schedule $t_1 > t_2 > \dots > t_L > 0$.
 - (2) Choose an $\mathbf{k}^{(1,1)}$, a set of time-points after screening $\mathbf{S}_{\mathbf{k}}^{(1,1)}$ based on $\mathbf{k}^{(1,1)}$ and total number of iterations N .
 - (3) For $l \in \{1, \dots, L\}$,
 - For $i \in \{1, \dots, J-1\}$,
 - (a) calculate $\pi(\mathbf{k} | \mathbf{y})$ for all $\mathbf{k} \in N_{\text{screen}}(\mathbf{k}^{(1,1)})$,
 - (b) select \mathbf{k}^- , and \mathbf{k}^+ from $\Gamma^-, \Gamma_{\text{screen}}^+$ with probabilities $\pi(\cdot | \mathbf{y})^{1/t_i}$,
 - (c) select $\mathbf{k}^{i+1,l}$ from $\{\mathbf{k}^-, \mathbf{k}^+\}$ with probabilities $\{\pi(\mathbf{k}^- | \mathbf{y})^{1/t_i}, \pi(\mathbf{k}^+ | \mathbf{y})^{1/t_i}\}$.
 - (d) update the set of variables considered to $\mathbf{S}_{\mathbf{k}}^{(i+1,l)}$ to be union of time-points in $\mathbf{k}^{i+1,l}$ and top M_n time-points according to $\{|r_{\mathbf{k}^{i+1,l}}' \Omega_j|, j = 2, \dots, T\}$.
-

Calculation of the Marginal Likelihood

Closed form expressions for posterior arrangement probabilities based on modified peMoM priors and modified piMoM priors are not available. We estimate the posterior arrangement probabilities using Laplace approximations, given by

$$m_{\mathbf{k}}(\mathbf{y}) = (2\pi)^{|\mathbf{k}|/2} \pi(\mathbf{y} | \hat{s}_{\mathbf{k}}) \pi(\hat{s}_{\mathbf{k}}) |G(\hat{s}_{\mathbf{k}})|^{-1/2}, \quad (9)$$

where $\hat{s}_{\mathbf{k}}$ is MAP of $s_{\mathbf{k}}$, $G(\hat{s}_{\mathbf{k}})$ is the Hessian of the negative log posterior density

$$g(s_{\mathbf{k}}) = -\log \pi(\mathbf{y} | s_{\mathbf{k}}) - \log \pi(s_{\mathbf{k}}),$$

evaluated at $\hat{s}_{\mathbf{k}}$. Following Shin et al. (2018), we use the limited memory version of the Broyden–Fletcher–Goldfarb–Shanno optimization algorithm (L-BFGS) (Liu and Nocedal (1989)) to find the MAP.

With this Laplace approximation of the arrangements probabilities, we utilize the stochastic algorithm discussed earlier to search the arrangement space to complete our posterior analysis. We report two summaries of our posterior analysis - (i) the highest posterior probability arrangement which is defined as the arrangement having the highest posterior probability among all visited arrangements, and (ii) the posterior probability for a spike at time point t which is defined as the sum of posterior probabilities of all arrangements that have a spike at time t . Since we have the complete model prior specification, and corresponding computational framework for posterior analysis in place, we are in a position to investigate the empirical performance of the proposed methodology.

2.3. Choice of the decay parameter γ in (2)

In literature, there are two common methods for estimating the decay parameter $\gamma \in (0, 1)$ in (2), that controls the rate of exponential decay of the calcium concentration. (i) Pnevmatikakis et al. (2013), Friedrich and Paninski (2016), and Friedrich, Zhou and Paninski (2017) propose to select the exponential decay parameter γ based on the auto-covariance function. We refer the reader to Friedrich, Zhou and Paninski (2017) and Pnevmatikakis et al. (2016) for additional details. (ii) Alternatively, Jewell and Witten (2018) advise choosing a segment $y_{a:b}$ manually first if it demonstrates exponential decline upon visual inspection.. Next, they estimate γ by

$$\hat{\gamma} = \arg \min_{\gamma \in (0,1)} \left\{ \min_{c_a, c_t = \gamma c_{t-1}, t=a+1, \dots, b} \left\{ \frac{1}{2} \sum_{t=a}^b (y_t - c_t)^2 \right\} \right\}.$$

Numerical optimization can be used to accomplish this.

3. Simulation Studies

In this section, we use simulated data to demonstrate the performance advantages of the proposed non local prior based methodologies over two competing frequentist approaches:

(i). The L_1 proposal in Friedrich and Paninski (2016) and Friedrich (2017), which involves a single tuning parameter λ . These approaches solve the optimization problem:

$$\min_{c_1, \dots, c_T, s_2, \dots, s_T} \left\{ \frac{1}{2} \sum_{t=1}^T (y_t - c_t)^2 + \lambda |c_1| + \lambda \sum_{t=2}^T |s_t| \right\} \quad \text{subject to} \quad s_t = c_t - \gamma c_{t-1} \geq 0, \quad (10)$$

where the hyper-parameter λ is fixed via cross-validation.

(ii). The state-of-the-art L_0 proposal in Jewell et al. (2019), which too involves a single tuning parameter λ , that poses the following optimization problem:

$$\min_{c_1, \dots, c_T, s_2, \dots, s_T} \left\{ \frac{1}{2} \sum_{t=1}^T (y_t - c_t)^2 + \lambda \sum_{t=2}^T \delta(s_t \neq 0) \right\}, \quad (11)$$

where $\delta(\cdot)$ is the Dirac delta measure, and the hyper-parameter λ is again fixed via cross-validation.

We measure performance in spike detection of each method based on several criteria: (i) accuracy, (ii) sensitivity, (iii) specificity, and (iv) false discovery rate. To that end, suppose c_1, c_2, \dots, c_T denote the true calcium concentration observed over time $t = 1, 2, \dots, T$, and we define $s_t = c_t - \rho c_{t-1}, t = 2, \dots, T$. Then, we can define

$$\begin{aligned} \text{Accuracy} &= \frac{1}{T-1} \left[\sum_{t=2}^T \left\{ \delta(s_t > 0, \hat{s}_t > 0) + \delta(s_t = 0, \hat{s}_t = 0) \right\} \right] \times 100\% ; \\ \text{Sensitivity} &= \frac{\sum_{t=2}^T \delta(s_t > 0, \hat{s}_t > 0)}{\sum_{t=2}^T [\delta(s_t > 0, \hat{s}_t > 0) + \delta(s_t > 0, \hat{s}_t = 0)]} \times 100\% = \frac{\sum_{t=2}^T \delta(s_t > 0, \hat{s}_t > 0)}{\sum_{t=2}^T [\delta(s_t > 0)]} \times 100\% ; \\ \text{Specificity} &= \frac{\sum_{t=2}^T \delta(s_t = 0, \hat{s}_t = 0)}{\sum_{t=2}^T [\delta(s_t = 0, \hat{s}_t = 0) + \delta(s_t > 0, \hat{s}_t = 0)]} \times 100\% = \frac{\sum_{t=2}^T \delta(s_t = 0, \hat{s}_t = 0)}{\sum_{t=2}^T [\delta(\hat{s}_t = 0)]} \times 100\% ; \\ \text{False discovery rate (FDR)} &= \frac{\sum_{t=2}^T \delta(s_t = 0, \hat{s}_t > 0)}{\sum_{t=2}^T [\delta(\hat{s}_t > 0)]} \times 100\% ; \end{aligned} \quad (12)$$

where $\delta(\cdot)$ is the Dirac delta measure, and we favour larger values of true spike detection rate and smaller values of false spike detection rate. Further, unlike the competing frequentist penalization methods, our proposed non local prior based approaches also yield (i) posterior probability associated with the maximum a posteriori arrangement of spikes and lack thereof, and (ii) posterior probability for a spike at each location of the spike train.

Table 1. Accuracy, sensitivity, and specificity for different methods averaged over 50 simulated data sets for $\gamma = 0.96, \sigma = 0.15$ and varying values of $T \in \{2000, 2500\}$.

	$T = 2000$				$T = 2500$			
	Accuracy	Sensitivity	Specificity	FDR	Accuracy	Sensitivity	Specificity	FDR
iMOM	99.97	97.93	99.99	00.00	99.98	98.12	99.99	00.00
eMOM	99.98	98.07	100.00	00.00	99.98	98.12	100.00	00.00
L_0	99.98	98.17	99.99	00.00	99.98	98.68	99.99	00.00
L_1	97.18	100.00	97.15	76.39	97.17	1.00	97.14	77.27

Based on Jewell et al. (2019), we generate 50 simulated data sets according to (2) with parameter settings $\gamma \in \{0.96, 0.98\}, T \in \{2000, 2500\}, \sigma = 0.15$, and $s_t \stackrel{i.i.d.}{\sim} \text{Poisson}(0.01)$. On each simulated data set, we compare our methodology with the two competing methods with respect to the performance metric delineated earlier. The decay parameter γ is estimated by the methods described in 2.3. The L_0

Table 2. Accuracy, sensitivity, and specificity for different methods averaged over 50 simulated data sets for $\gamma = 0.98$, $\sigma = 0.15$ and varying values of $T \in \{2000, 2500\}$.

	$T = 2000$				$T = 2500$			
	Accuracy	Sensitivity	Specificity	FDR	Accuracy	Sensitivity	Specificity	FDR
iMOM	99.97	97.20	99.99	00.00	99.98	98.12	99.99	00.00
eMOM	99.97	97.20	99.99	00.00	99.97	98.12	99.99	00.00
L_0	99.98	98.10	99.99	00.00	99.98	98.53	99.99	00.00
L_1	96.31	100.00	96.27	81.91	96.35	100.00	96.31	79.67

(11) and L_1 (10) regularised approaches are utilized with a hyper parameter tuning step involving cross-validation. For the inverse moment prior and the exponential moment prior based approaches, we utilize the S5 algorithm with a Bernoulli-Uniform prior on the spike arrangement space. To ensure the stability of the stochastic search based algorithm, we utilize 10 random starting points and a temperature schedule of $\{0.4, 0.5, \dots, 1.0\}$. Also, the stochastic search was distributed in 50 cores in order to expedite the calculations.

In Tables 1 and 2, we present the performance metrics for the spike detection task averaged over 50 simulated data sets, corresponding to our non-local prior based methods as well as the penalised likelihood based frequentest methods. All four methods perform extremely well in detecting true spikes, as depicted by comparably high sensitivity and specificity figures across all simulation setups. However, the frequentest method based on L_1 regularization results in high number of false spike discovery, whereas the L_0 regularised method and the non-local prior based methods almost never discovered a false spike across the repeated simulations. This provides compelling empirical evidence that, our non-local prior based proposals lead to substantial improvements over the previous proposal based on L_1 regularization, and enjoys comparable estimation accuracy to the state-of-the-art L_0 proposal. Furthermore, contrary to the optimization based frequentest approaches, our methodologies yields automatic uncertainty quantification associated with the spike train inference. In particular, we provide the probability corresponding to the highest posterior probability arrangements of spikes and lack there of. Moreover, we provide the posterior probability of a spike at each time-point in the spike-train.

In particular, for the sake of this presentation, we focus on a single simulated data set generated with $\gamma = 0.96$, $T = 2000$, $\sigma = 0.15$. For this data set, the L_0 , inverse moment prior, and exponential moment prior based approaches identified exactly same number of spikes at very similar and visually reasonable time points, presented as red dots in figure 3. But, as observed in much of previous literature (Jewell et al. (2019)), the L_1 regularised approach results in many, typically small in magnitude, false spike discoveries. Further, we observe that the maximum a posteriori estimates corresponding to the inverse moment and exponential moment priors has posterior probabilities equal to 0.9999 and 0.9997 respectively. The posterior probability of a spike at the different time point corresponding to the inverse moment and exponential moment prior based approaches are presented as red dots in the two panels in figure 2.

4. Application to Calcium Imaging data sets

Action potential derivation from neuronal calcium signals is complicated due to the lack of simultaneous measurements of action potentials and

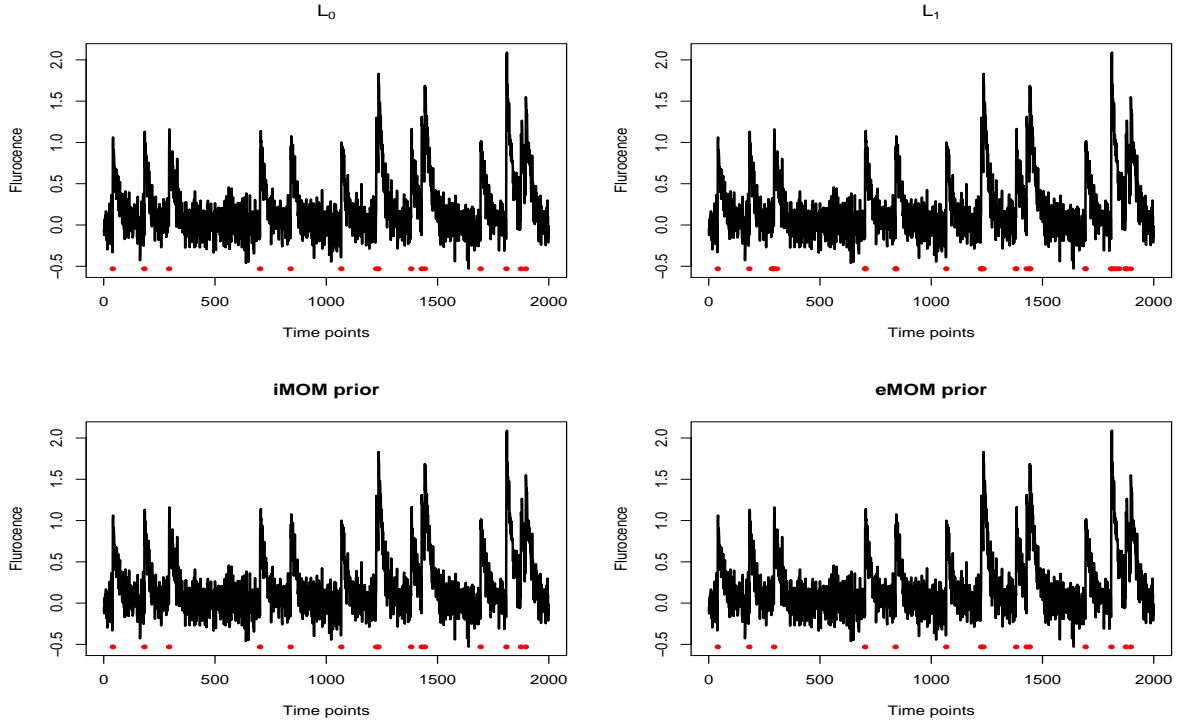


Figure 1. Simulated data: One particular simulated data generated with specifications $\gamma = 0.96$, $T = 2000$, $\sigma = 0.15$. Each panel displays the DF/F -transformed fluorescence (in black lines), the estimated spikes by the red dots. The four panels display results obtained via the L_0 , L_1 , $iMOM$, $eMOM$ based methods respectively.

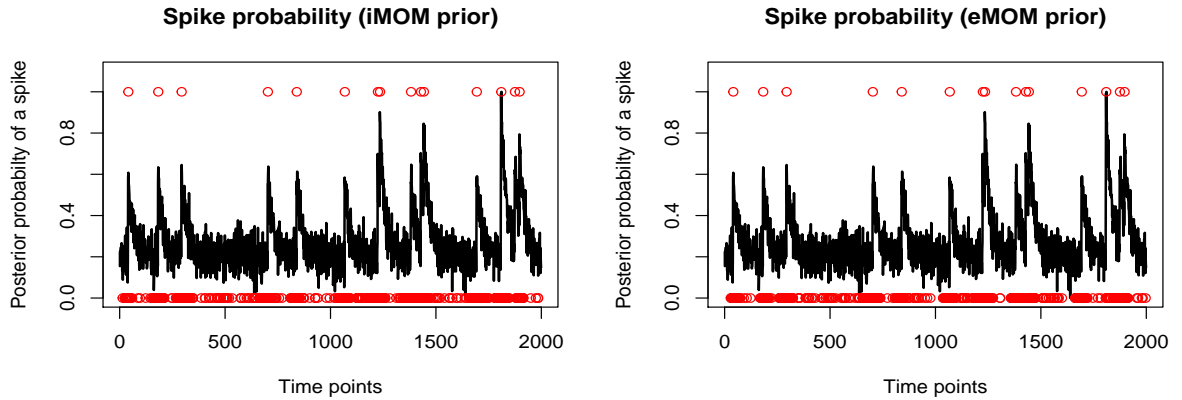


Figure 2. Simulated data: One particular simulated data generated with specifications $\gamma = 0.96$, $T = 2000$, $\sigma = 0.15$. The two panel displays the centered and scaled DF/F -transformed fluorescence re scaled to $(0, 1)$ (in black lines) and the posterior probabilities of spikes at different time points by red dots, for the $iMOM$, $eMOM$ based methods respectively.

calcium signals. Rupprecht (2021) compiled a huge and varied database (github.com/HelmchenLabSoftware/Cascade) from publicly available and newly performed recordings in *zebrafish* and *mice*, consisting of 298 neurons' combined record-

ings over more than 35 hours, and encompassing a wide range of cell types, calcium markers, and signal-to-noise ratios. By performing simultaneous electrophysiological recordings and calcium imaging in both *zebrafish* and *mice*, Rupprecht (2021) was able to broaden the range of data sets that were available. In *zebrafish*, using the synthetic calcium indicators Oregon Green BAPTA-1 (OGB-1) and Cal-520 as well as the genetically encoded calcium indicator GCaMP6f, a total of 47 neurons in various telencephalic areas were recorded in the juxtacellular configuration in an explant preparation of the entire adult brain.. In head-fixed *mice*, using the genetically encoded indication R-CaMP1.07, recordings were made in the hippocampus area CA3 while the subject was under anesthesia. Further, Rupprecht (2021) examined freely available data sets and gathered information from raw movies. There were originally 157 neurons available, down from a total of 193 after thorough quality screening. In addition to their own recordings, Rupprecht (2021) compiled 27 data sets with a combined total of 495,077 spikes and ~ 38 hours of recording from 298 neurons, eight calcium indicators, and nine different brain areas in two species..

The data sets showed significant differences in recording times, imaging frame rates, and spike rates. Typical spike rates spanned more than an order of magnitude, ranging from 0.4 Hz to 11.6 Hz, and frame rates varied between 7.7 Hz and > 160 Hz . Using regularized deconvolution, Rupprecht (2021) computed the linear $\Delta F/F$ kernel evoked by the average spike and discovered that, even for data from the same calcium indicator, the area under the kernel curve varied significantly between data sets and was significantly smaller for data sets with inhibitory neurons. The issue faced by any algorithm that is supposed to analyze the data is shown by the fact that kernels displayed significant variance even among neurons within the same data set.

To demonstrate the performance the proposed non local priors based approaches in spike estimation estimation and uncertainty quantification, we present the results for two particular data sets - one is a calcium fluorescence observed in mice Theis (2016), and the other for zebra fish (Rupprecht (2021)). The L_0 (11) and L_1 (10) regularised approaches are utilized with a hyper parameter tuning step involving cross-validation. For the inverse moment prior and the exponential moment prior based approaches, we utilize the S5 algorithm with a Bernoulli-Uniform prior on the spike arrangement space. To ensure the stability of the stochastic search based algorithm, we utilize 10 random starting points and a temperature schedule of $\{0.4, 0.5, \dots, 1.0\}$. Also, the stochastic search was distributed in 50 cores in order to expedite the calculations.

4.1. *Application to Theis (2016) data*

First, we consider a data set that consists of simultaneous calcium imaging of *mice*, originally presented in Theis (2016), and compiled in Rupprecht (2021) as a part of the large and diverse database. The black lines in the figure 5 presents the first 28 minutes of calcium trace recording from cell 10 of mice 2 for, which expresses OGB-1. The data are measured for a total of 2000 time-steps. As earlier, the raw fluorescence traces are DF/F transformed with a 20% percentile filter (Friedrich (2017)).

For this data set, the L_0 , L_1 , inverse moment prior, and exponential moment prior based approaches identified 15, 38, 14 and 14 spikes respectively, presented as red dots in figure 3. The spikes corresponding to the the L_0 , inverse moment prior, and exponential moment prior based approaches appear at similar and visually reasonable time points. But, as observed in our simulation studies as well as much of previous literature (Jewell et al. (2019)), the L_1 regularised approach results in many, typically

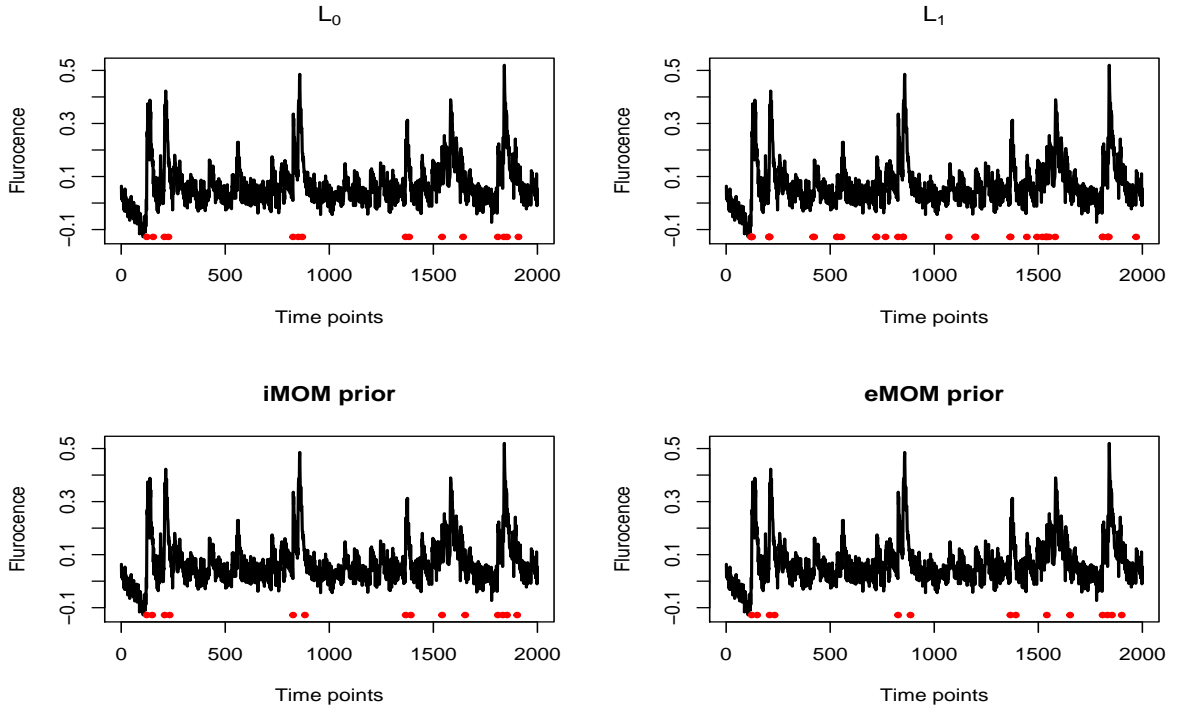


Figure 3. Mice data: The calcium fluorescence data from mice in Theis (2016). Each panel displays the DF/F -transformed fluorescence (in black lines), the estimated spikes by the red dots. The four panels display results obtained via the L_0 , L_1 , $iMOM$, $eMOM$ based methods respectively.

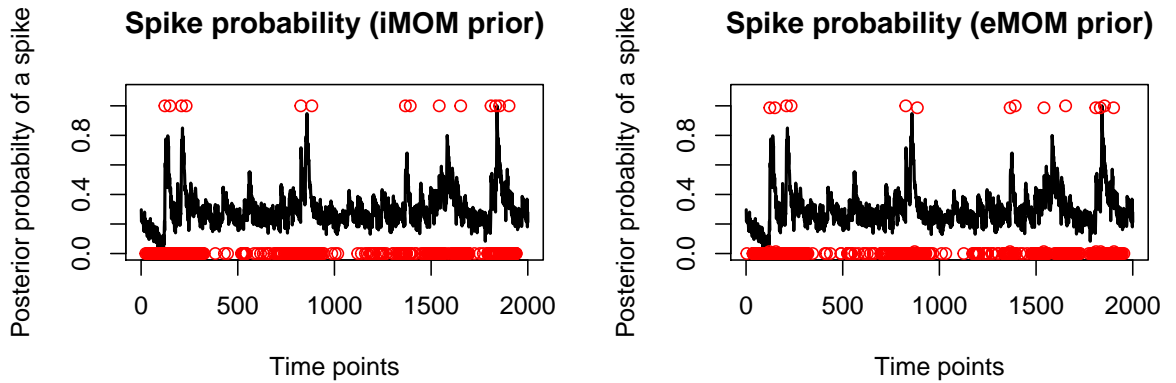


Figure 4. Mice data: The calcium fluorescence data from mice in Theis (2016). The two panel displays the centered and scaled DF/F -transformed fluorescence re scaled to $(0,1)$ (in black lines) and the posterior probabilities of spikes at different time points by red dots, for the $iMOM$, $eMOM$ based methods respectively.

small in magnitude, false spike discoveries. Unlike the penalised likelihood based procedures, our proposed methods provide complete uncertainty quantification regarding the spike train inference. In particular, the reported maximum a posteriori estimates corresponding to the inverse moment and exponential moment priors has posterior

probabilities equal to 0.986 and 0.999 respectively. Further, the posterior probability of a spike at the different time point corresponding to the inverse moment and exponential moment prior based approaches are presented as red dots in the two panels in figure 4.

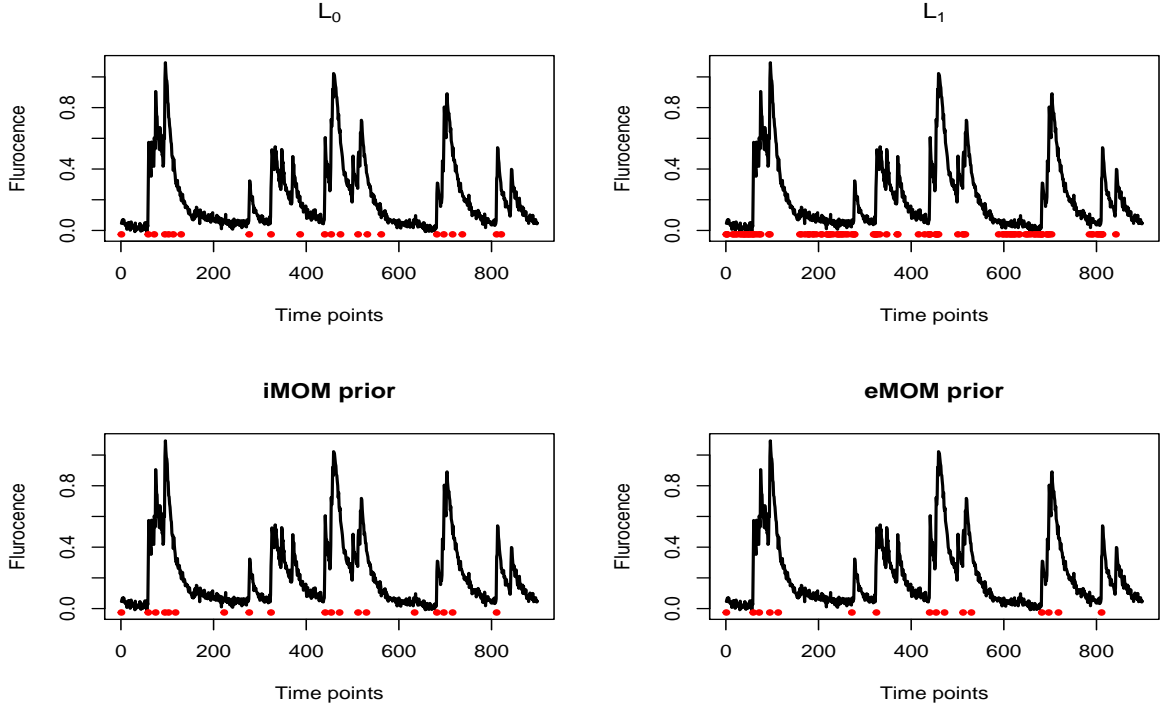


Figure 5. Zebra fish data: The calcium fluorescence data for Zebra fish in Rupprecht (2021). Each panel displays the DF/F -transformed fluorescence (in black line), the estimated spikes by the red dots. The four panels display results obtained via the L_0 , L_1 , *iMOM*, *eMOM* based methods respectively.

4.2. Application to Rupprecht (2021) data

Next, we consider a data set that consists of simultaneous calcium imaging of *zebrafish*, originally presented in Rupprecht (2021), as a part of a large and diverse database. The black lines in the figure 5 presents a 81 minute calcium trace recording from cell 4 of fish 2 for, which expresses OGB-1. The data are measured for a total of 900 time-steps. The raw fluorescence traces are DF/F transformed with a 20% percentile filter (Friedrich (2017)).

For this data set, the L_0 , L_1 , inverse moment prior, and exponential moment prior based approaches identified 22, 120, 19 and 16 spikes respectively, presented as red dots in figure 5. The spikes corresponding to the the L_0 , inverse moment prior, and exponential moment prior based approaches appear at similar and visually reasonable time points. But, as observed in our simulation studies as well as much of previous literature (Jewell et al. (2019)), the L_1 regularised approach results in many, typically small in magnitude, false spike discoveries. Unlike the penalised likelihood based procedures, our proposed methods provide complete uncertainty quantification regarding the spike train inference. In particular, the reported maximum a posteriori estimates

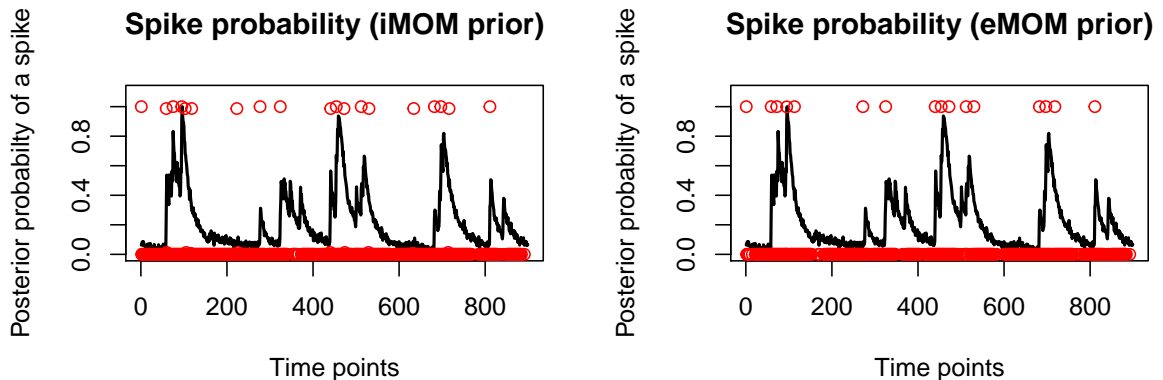


Figure 6. Zebra fish data: The calcium fluorescence data for Zebra fish in Rupprecht (2021). The two panel displays the centered and scaled DF/F -transformed fluorescence re scaled to $(0, 1)$ (in black lines) and the posterior probabilities of spikes at different time points by red dots, for the $iMOM$, $eMOM$ based methods respectively.

corresponding to the inverse moment and exponential moment priors has posterior probabilities equal to 0.987 and 0.998 respectively. Further, the posterior probability of a spike at the different time point corresponding to the inverse moment and exponential moment prior based approaches are presented as red dots in the two panels in figure 6.

5. Discussion

Recent advances in neuroscience have enabled researchers to measure the activities of large numbers of neurons simultaneously in behaving animals. Scientists have access to the fluorescence of each of the neurons that provides a first-order approximation to the neural activity over time. Determining a neuron's exact spike time is an important challenge that remains an active area of research within the field of computational neuroscience. This problem has recently been addressed using penalized likelihood methods (Jewell et al. (2019), Friedrich and Paninski (2016), Friedrich (2017)). In this paper, we proposed a new approach for this task based on a novel application of a mixture prior on spike variables that has a point mass at zero and a half non local density (Johnson and Rossell (2010)), in the popular auto-regressive model for calcium dynamics. Our proposals lead to substantial improvements over the previous proposal based on L_1 regularization, and enjoys comparable estimation accuracy to the state-of-the-art L_0 proposal, in simulations as well as on recent calcium imaging data sets. Notably, contrary to most optimization based frequentist approaches, our methodology yields automatic uncertainty quantification associated with the spike train inference.

One compelling direction for future enquiry includes positing a hierarchical Bayesian framework to simultaneously model multitude of spike trains arising from different neurons an animal interest. This will lead us to understand the complete neural response of the animal towards an external signal. Further, there is merit in attempting to carry out the spike train inference in online fashion, i.e, real time estimation and uncertainty quantification of spikes as the data arrives to a system, in order to improve its practical

applicability.

6. Data availability statement

All the data utilized in this study is freely available in:
github.com/HelmchenLabSoftware/Cascade.

Disclosure statement

The author reports there are no competing interests to declare.

Funding details

There was non external on internal funding for this work.

References

- Fan, e. a. (2008). Sure independence screening for ultrahigh dimensional feature space. *JRSS-B*.
- Friedrich, e. a. (2017). Fast online deconvolution of calcium imaging data. *Plos computational biology*.
- Friedrich, J. and Paninski, L. (2016). Fast active set methods for online spike inference from calcium imaging. In Lee, D., Sugiyama, M., Luxburg, U., Guyon, I., and Garnett, R., editors, *Advances in Neural Information Processing Systems*, volume 29. Curran Associates, Inc.
- Hans, C., Dobra, A., and West, M. (2007). Shotgun stochastic search for “large p” regression. *Journal of the American Statistical Association*, 102(478):507–516.
- Jewell, S. W., Hocking, T. D., Fearnhead, P., and Witten, D. M. (2019). Fast nonconvex deconvolution of calcium imaging data. *Biostatistics*, 21(4):709–726.
- Johnson, V. E. and Rossell, D. (2010). On the use of non-local prior densities in bayesian hypothesis tests. *Journal of the Royal Statistical Society. Series B (Statistical Methodology)*, 72(2):143–170.
- Johnson, V. E. and Rossell, D. (2012). Bayesian model selection in high-dimensional settings. *Journal of the American Statistical Association*, 107(498):649–660.
- Linderman, S., Adams, R. P., and Pillow, J. W. (2016). Bayesian latent structure discovery from multi-neuron recordings. In Lee, D. D., Sugiyama, M., Luxburg, U. V., Guyon, I., and Garnett, R., editors, *Advances in Neural Information Processing Systems 29*, pages 2002–2010. Curran Associates, Inc.
- Liu, D. C. and Nocedal, J. (1989). On the limited memory bfgs method for large scale optimization. *Mathematical Programming*, 45:503–528.
- Moral, e. a. (2006). Bayesian spike inference from calcium imaging data. *Journal of the Royal Statistical Society: Series B (Statistical Methodology)*.
- Nikooienejad, A., Wang, W., and Johnson, V. E. (2016). Bayesian variable selection for binary outcomes in high-dimensional genomic studies using non-local priors. *Bioinformatics*, 32(9):1338–1345.
- Nikooienejad, e. a. (2020). Bayesian variable selection for survival data using inverse moment priors. *Ann Appl Stat*.
- Pnevmatikakis EA, e. a. (2013). Bayesian spike inference from calcium imaging data.
- Pnevmatikakis EA, e. a. (2016). Simultaneous denoising, deconvolution, and demixing of calcium imaging data. *Neuron*.

- Pramanik, S., Johnson, V. E., and Bhattacharya, A. (2021). A modified sequential probability ratio test. *Journal of Mathematical Psychology*, 101:102505.
- Rupprecht, e. a. (2021). A database and deep learning toolbox for noise-optimized, generalized spike inference from calcium imaging. *Nat Neurosci*, 45:503–528.
- Shin, M., Bhattacharya, A., and Johnson, V. E. (2018). Scalable bayesian variable selection using nonlocal prior densities in ultrahigh-dimensional settings. *Statistica Sinica*, 28(2):1053–1078.
- Theis, e. a. (2016). Benchmarking spike rate inference in population calcium imaging. *Neuron*.
- Tibshirani, R. (1996). Regression shrinkage and selection via the lasso. *Journal of the Royal Statistical Society. Series B (Methodological)*, 58(1):267–288.
- Vogelstein, e. a. (2009). Spike inference from calcium imaging using sequential monte carlo methods. *Biophys J*.
- Vogelstein, e. a. (2010). Fast nonnegative deconvolution for spike train inference from population calcium imaging. *J Neurophysiol*.